Journal of Combinatorial Mathematics
and Combinatorial Computing
www.combinatorialpress.com/jcmcc

Combinatorial Press

Optimization of a near-infrared photothermally controlled nano-retarded release system for loading the anticancer drug adriamycin based on numerical simulation calculations

Lili Deng[1,✉], Xue Zhou[1]

[1] *Zhengzhou Technical College, Zhengzhou, Henan, 450121, China*

ABSTRACT
The aim of this study is to develop a near-infrared photothermally controlled nano-retarded release system loaded with the anticancer drug Adriamycin optimized based on numerical simulation calculations. Firstly, the instruments, agents and experimental methods for the preparation of self-assembled albumin-loaded nanoparticles were introduced.The cumulative absorption wavelengths of the albumin nanoparticles were investigated by UV and IR spectroscopy, and it was found that the maximal absorption wavelengths of DOX and BDC were distributed at 487 nm and 435 nm, and that the UV maximal absorption wavelength of CUR was 435 nm.In the in vitro slow-release performance, it was found that the cumulative release rate of DOX reached 97.36% when pH 5.0 was used, and that when CUR was used, the cumulative release rate of DOX reached 97.36%. The cumulative release rate of DOX reached 97.36% at pH 5.0, while it was only 59.15% and 30.81% at pH 6.0 and 7.0. The cumulative release rates of CUR at the three pH values were 58.69%, 29.98% and 16.81%, respectively, which were basically the same trend of the retardation curves of the two drugs. The nanoparticles degraded morphology showed the widest and narrowest particle size distribution in PBS buffer solution at pH=5.0 and 7.0, respectively. The loading capacity of the optimized model showed good consistency of effect on measured (11.03%) and predicted (10.87%) values.The photothermal conversion experiments of DOX nanoliposomes were found to have concentration and time dependent photothermal conversion effects. In this paper, from the optical characterization of albumin drug-carrying nanoparticles, it was found that UV light was able to excite PFNSNO for photodynamic therapy as well as NO release through the fluorescence resonance energy transfer process.

Keywords: Numerical simulation calculations; Nano-slow-release system; Albumin-loaded nanoparticles; Anti-cancer drug Adriamycin

1. Introduction

Cancer is known as a malignant tumor, which is triggered by malignant proliferation of cells and is invasive and metastatic [1]. According to global cancer statistics, liver cancer is the sixth most common

✉ Corresponding author.
E-mail address: zzybiodll@126.com (L. Deng).
Received 05 March 2024; Revised 10 May 2024; Accepted 05 December 2024; Published Online 15 April 2025.
DOI: 10.61091/jcmcc127a-298

cancer and the third most common cause of cancer-related deaths worldwide [2]. The incidence of hepatocellular carcinoma is on the rise globally, with hepatocellular carcinoma accounting for a high proportion of primary liver cancers [3]. The incidence and mortality rates in China remain at a high level, which imposes a heavy burden on society and families.

In clinical work, ablation and TACE are common modalities for the treatment of hepatocellular carcinoma, which have the advantages of fewer toxic side effects and higher therapeutic efficiency [4-6]. However, there are limitations and contraindications to treatments such as hyperthermia ablation and TACE, so other treatments are needed to complement them [7-8]. Novel optical treatments such as photodynamic therapy (PDT) and photothermal therapy (PTT) have the advantages of being minimally invasive, low toxicity, and non-resistant [9-10]. However, the characteristics of phototherapeutic agents such as lower photostability, high scattered light loss, and hypoxia in the tumor microenvironment limit their application in the field of PDT and PTT [11-12]. Seeking strategies to combine optical therapeutic methods with traditional therapies to develop a diagnostic and treatment system that integrates disease diagnosis, targeted drug delivery, and multiple therapeutic modalities provides a new idea to address the problems of low anti-tumor efficiency, drug resistance, and high effects on normal tissue cells [13-16].

In this study, we optimized the design of near-external infrared thermally controlled nanodelivery system for adriamycin-loaded slow-release based on numerical simulation calculations. The experimental process of albumin-loaded drug nanoparticles is designed and the preparation process of self-assembled albumin-loaded drug nanoparticles is proposed. Then the processes of characterization of albumin drug-loaded nanoparticles, in vitro slow-release performance and morphological characterization of nanoparticles after degradation were carried out to determine the optimal preparation process of albumin drug-loaded nanoparticles. The thermal conductivity properties and drug diffusion process of the nanomaterials were simulated and analyzed by photothermal conversion test and optical property characterization of DOX nanoliposomes, and provided a new strategy for the efficient delivery of anticancer drugs.

2. Preparation of self-assembled albumin drug-carrying nanoparticles

2.1. Instruments and reagents

2.1.1. Instruments. Particle Size and Surface Potential Meter, Transmission Electron Microscope, UV & Visible Spectrophotometer, Fluorescence Spectrophotometer, Electronic Balance, Rotary Vaporizer, Temperature-Controlled Electrothermal Magnetic Stirrer, Ultra-pure Water Meter, Digital Thermometer Recorder, Near-infrared Laser Meter, Constant Temperature Oscillator, Ultrasonic Cell Crusher, Freeze-dryer, Refrigerated Centrifuge, Ultrasonic Cleaner.

2.1.2. Reagents. Human serum albumin, adriamycin hydrochloride, indocyanine green, fetal bovine serum, α-DMEM cell culture medium, RPMI 1640 cell culture medium, trypsin, penicillin-streptomycin, dialysis bag, glutathione Other unspecified chemicals and reagents were purchased from Sinopharm Chemical Reagent Co. The chemical reagents used in the experiments were analytically pure or chromatographically pure without further purification.

2.2. Experimental methods for albumin drug-loaded nanoparticles

1) Preparation of hydrophobic adriamycin (DOX). 100 mg of adriamycin hydrochloride (DOX-HCl) was taken and weighed precisely. Dissolve in dimethyl sulfoxide (DMSO), formulate a solution of 20 mg/mL, add triethylamine (TEA) dropwise, (TEA:DOX-HCl = 2:1, mol/mol), stirring at room temperature and away from light for 12 h. At the end of the reaction, the reaction solution was placed in a dialysis bag (Mw = 3.5 kDa), dialyzed in deionized water for 48 h, centrifuged, and precipitate was collected. The

precipitate was washed several times with deionized water and freeze-dried to obtain hydrophobic adriamycin (DOX) [17].

2) Nanoparticle preparation and prescription optimization. Albumin drug-carrying nanoparticles were prepared by a modified reduction-self-assembly method [18]. 10 mg of ICG was taken and dissolved in 1 mLDMSO to formulate 10 mg/mL of ICG mother liquor. In the same method, 10mg/mL of hydrophobic DOX masterbatch was prepared. 20mg of HSA was dissolved in 2mL of phosphate buffer salt solution (pH 8.0), 6mgGSH was added, and stirred at room temperature for 0.5h. 100μL of hydrophobic DOX and ICG masterbatch was added, and the stirring was continued for 0.5h. 2mL of counter-solvent ethanol was added and then stirred for 0.5h to obtain the co-loaded DOX and ICG albumin nanoparticles mixed solvent dispersion. The ethanol was immediately removed by spin distillation, and the remaining ethanol and DMSO were removed by dialysis (Mw=100kDa) for 24h.

3) Evaluation of physicochemical properties of nanoparticles. The DI@HSA NPs prepared as described above were taken and diluted with ultrapure water to a suitable concentration, and then the particle size and surface potential of the DI@HSA NPs were determined using a particle size and surface potential meter. In addition, the prepared and obtained DI@HSA NPs were diluted 10 times with deionized water, slowly dripped onto a copper mesh, dried at room temperature, stained with 2% (w/v) phosphotungstic acid, excess phosphotungstic acid was absorbed by filter paper, and the morphology and size of DI@HSA NPs were observed by transmission electron microscopy (TEM).

4) Nanoparticle spectral scanning. Each drug-carrying nanoparticles and free ICG, diluted to the appropriate concentration with ultrapure water, were scanned by UV & VIS spectrophotometer at 400-900 nm to obtain the UV absorption spectra of DI@HSA NPs, ICG@HSA NPs and free ICG. The DI@HSA NPs and free DOX fluorescence spectra were also obtained by fluorescence spectrophotometer by scanning with a fixed excitation wavelength of 505 nm and a step size of 5 nm.

5) Nanoparticle drug loading and encapsulation rate. The ICG and DOX contents were determined by UV&Vis spectrophotometry and fluorescence spectrophotometry, respectively.

Preparation of ICG standard curve: Take the ICG mother liquor prepared by 2-2-2, and dilute it to 0.5, 0.75, 1.0, 2.0, 4.0 and 5.0 $\mu g \cdot mL^{-1}$ with mixed solvent (ethanol: water=9:1, v/v) respectively. The absorption value (A) at the maximum absorption wavelength of 792 nm was determined by UV-visible spectrophotometer, and the ICG standard curve was plotted with the absorption value (A) as the vertical coordinate and the ICG concentration C($\mu g \cdot mL^{-1}$) as the horizontal coordinate.

Preparation of DOX standard curve: Take the DOX master batch prepared by 2-2-2 and dilute it to 0.1, 0.25, 0.5, 1.0, 2.0 and 4.0 $\mu g \cdot mL^{-1}$ respectively with mixed solvent (ethanol: water=9:1, v/v). Fluorescence spectrophotometer was used to determine the DOX absorption value (A). The excitation wavelength was set at 505 nm, the emission wavelength at 565 nm and the step size at 5 nm, and the DOX standard curve was plotted with the absorption value (FL) as the vertical coordinate and the DOX concentration C($\mu g \cdot mL^{-1}$) as the horizontal coordinate.

Determination of drug loading and encapsulation rate: Take DI@HSANPs aqueous dispersion 50 μL, extract and dilute 50 times with mixed solvents, sonicate in water bath for 30 min, determine the ICG concentration by UV & VIS spectrophotometry, and determine the DOX concentration by fluorescence spectrophotometry. The drug loading (DL%) and encapsulation rate (EE%) were calculated by substituting into equations (1) and (2), respectively:

$$DL\% = C \times V / W_{NPs} \times 100\% \quad (1)$$

$$EE\% = C \times V / M_{Drug} \times 100\% \quad (2)$$

Where: C is the drug concentration in the drug-loaded nanoparticles, V is the volume of drug-loaded nanoparticles after dialysis, W_{NPs} is the mass of the drug-loaded nanoparticles, and M_{Drug} is the amount of drug administered.

6) Determination of ICG stability in nanoparticles. The absorbance values of DI@HSANPs, ICG@HSANPs and free ICG aqueous solution (CicG: 8.75 $\mu g \cdot mL^{-1}$) at 792 nm were measured continuously over a period of 1 week using UV-visible spectrophotometry [19], and the aqueous stability of ICG in albumin nanoparticles was evaluated based on the change in absorbance values.
7) NIR photothermal conversion efficiency of nanoparticles. Each sample solution was added to a 1.5 mL plastic tube (CıcG: 7.5 $\mu g \cdot mL^{-1}$) and irradiated by near-infrared laser (808 nm, 1.5 $W \cdot cm^2$, 5 min), and the temperature change of each solution was recorded every 30 s with a digital thermometer for examining the near-infrared photothermal conversion efficiency of the albumin drug-carrying nanoparticles.After completion of the 5-min irradiation, the DI@HSANPs and free ICGPBS solution was cooled down to room temperature. After 5 min of irradiation, the DI@HSANPs and free ICGPBS solutions were cooled to room temperature and irradiated again for 5 min, and the temperatures at each time point were recorded with a digital thermometer, which was used to study the photothermal stability of DI@HSANPs and free ICG.
8) Examination of nanoparticle stability. For 1 week, the particle size of the aqueous solution of DI@HSANPs was determined every other day using a particle size and surface potential meter, and the change in particle size was recorded. Next, DI@HSANPs were dispersed into DMEM, 10% fetal bovine serum, and pH 7. 4 PBS solution, and the clarification was observed daily and recorded for 7 days. Finally, 10-fold DMEM was used to simulate the internal environment of the organism, and the changes in the particle size of DI@HSANPs were measured and recorded over 48h.
9) In vitro release studies of nanoparticles. The dialysis bag method was used to study the in vitro release behavior of DOX from DI@HSANPs and DOX@HSANPs. Dialysis bags (MWCO=3.5 kDa, Coox=30 $\mu g \cdot mL^{-1}$) containing ImL of free DOX, DI@HSANPs and DOX@HSANPs aqueous dispersion solution, respectively, were sealed and then diffused into plastic tubes containing 25 mL of PBS buffer solution at pH 7.4 (buffer solution containing 0.2% Tween 80, v/v), which were placed in a thermostatic shaker for oscillation (37 $^{\circ}C$ at 100 rpm) and sampled at 0.5, 1, 2, 4, 8, 12, 24, and 48 h. The 25 mL of release medium was replaced again after each sampling.

3. Results and discussion

3.1. Characterization of nanoparticles

Figure 1 shows the UV spectra of BDC nanoparticles. Since the maximum absorption wavelength of DOX is at 487 nm and the maximum absorption wavelength of CUR is at 435 nm, the maximum absorption wavelength of BDC is at 507 nm, and there is a shoulder peak at 370 nm, which is close to the maximum absorption wavelengths of DOX and CUR, respectively, suggesting that both of them have been crosslinked with di-(1,6-dipropargyl) hexane-1,6-dipropargyl acid ester to form BDC. The peaks of BDC were broader due to the shift of the peak position after the bonding of DOX and CUR.

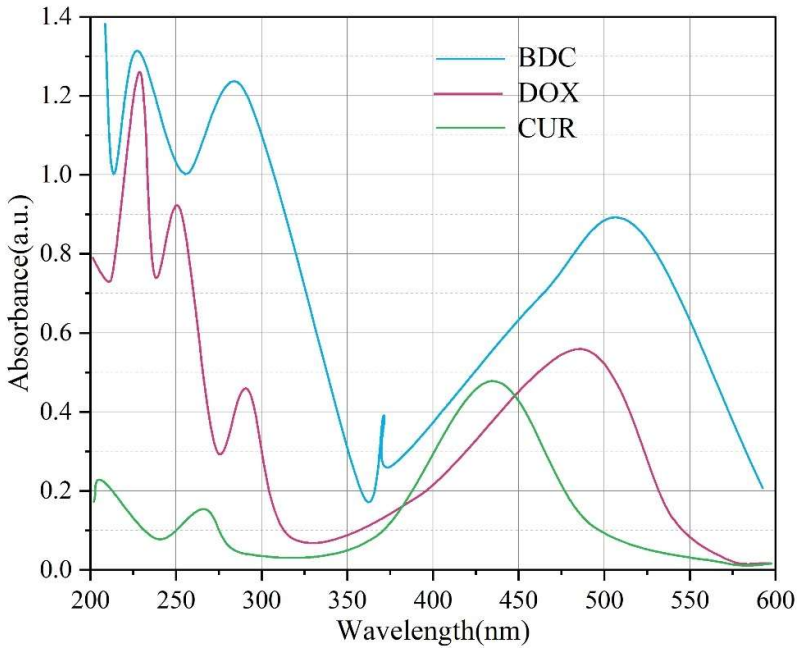

Fig. 1. BDC nanoparticles of ultraviolet spectrum

The IR spectra of the BDC polyprecursors are shown in Fig. 2. The characteristic peaks of functional groups such as ester group (-COOR), alkynyl group (-C≡C) and carbonyl group (-C=O) are visible for hexane-1,6-dipropynoic acid diester (Ester). The characteristic absorption peak for C≡C is at 2131 cm-1. There is a strong stretching vibration of (≡C-H) at 3277 cm-1, a characteristic absorption peak of C=O at 1747 cm-1, and characteristic peaks of C-O-C at 1074 cm-1 and 1307 cm-1.In the infrared spectra of BDC, there is an absorption peak of -OH at 3497 cm-1, and due to the conjugation effect, there are characteristic peaks of the unsaturated ketone group of C=O at 1703 cm-1, and a characteristic peak of α- and carbonyl groups of C=O at 1603 cm-1, and a characteristic peak of C=O at 1603 cm-1. 1603 cm-1 is the characteristic peak of α,β-unsaturated ketone, and 1363 cm-1 and 1244 cm-1 are the characteristic peaks of the allylic ether bond in BDC. It can be seen that the peaks of alkyne and ether bonds disappeared in BDC, and the alkyne group and phenolic hydroxyl group polymerized to form the alkenyl ether bond by click reaction, which further indicates that the reaction synthesized BDC.

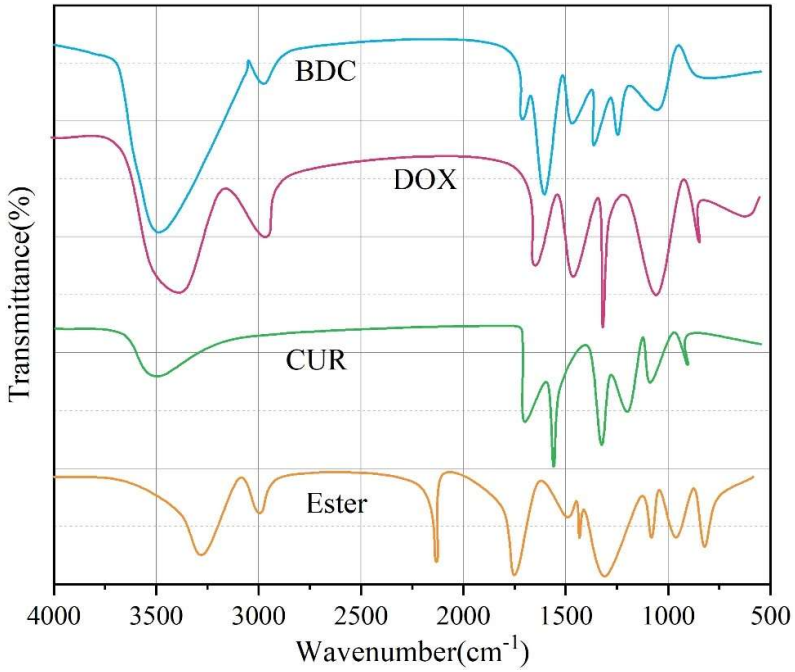

Fig. 2. The infrared light spectrum of the BDC polymer

The particle size distribution of the BDC nanoparticles is shown in Fig. 3.The average hydrated diameter of the BDC nanoparticles measured by the particle size meter was 250 nm, and the PDI was 0.1324, which indicated that the homogeneity of the fabricated nanoparticles was good.

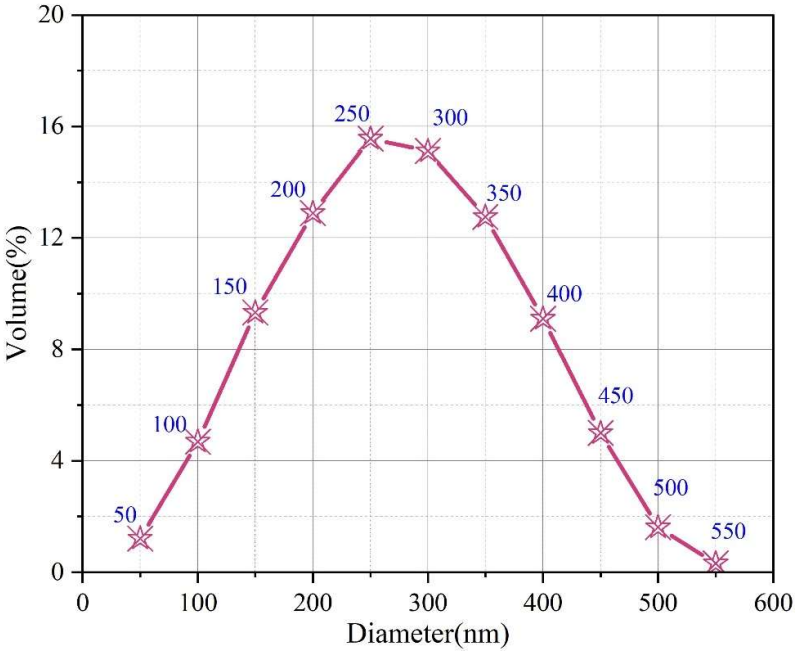

Fig. 3. Particle size distribution of BDC nanoparticles

3.2. In vitro slow release properties

The in vitro release curves of adriamycin and curcumin are shown in Fig. 4, where (a) and (b) represent adriamycin and curcumin, respectively.The slow-release curves of DOX can be seen that: the cumulative release rate varied considerably at different pH conditions during 96 h. DOX was basically released completely at pH 5.0 with a cumulative release rate of 97.36%, at pH 6.0 with a cumulative

release rate of 59.15%, and at pH 7.0 with a cumulative release rate of 30.81%. At pH 6.0, the cumulative release rate was 59.15%, and at pH 7.0, the cumulative release rate was 30.81%. The slow release curve of CUR showed that the cumulative release rate of CUR was 58.69%, 29.98% and 16.81% at pH 5.0, 6.0 and 7.0, respectively. The trend of the slow-release curves of the two drugs was basically the same, and the cumulative release rate was significantly dependent on both pH and time.

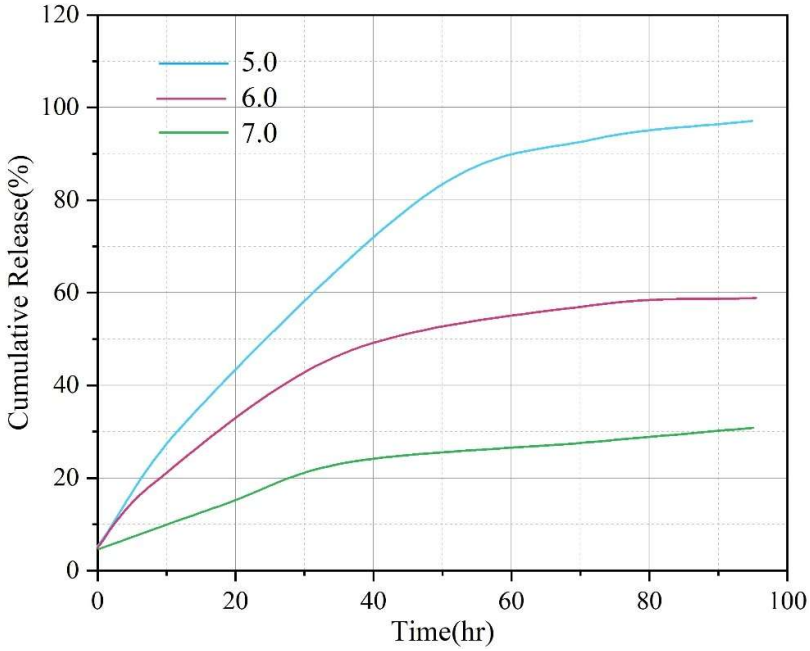

(a) DOX

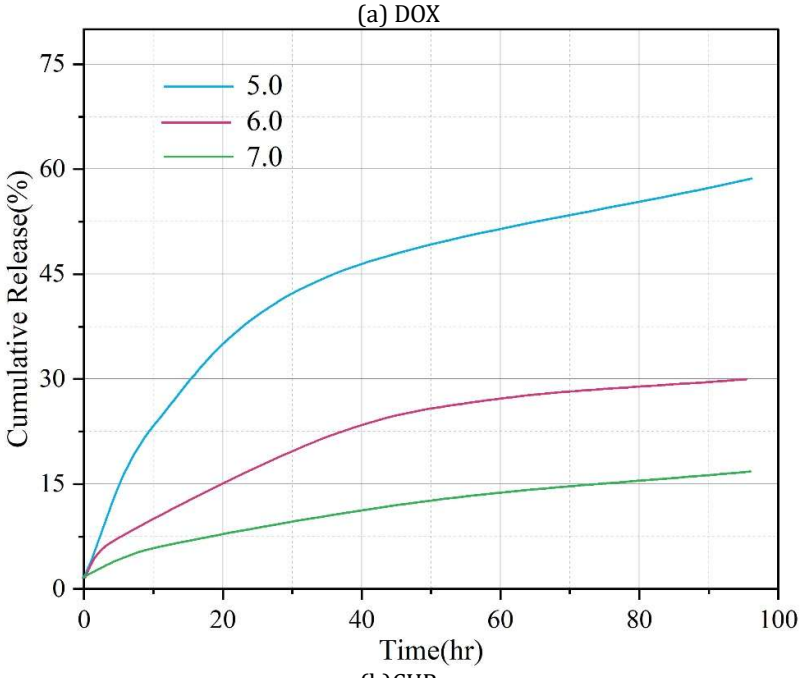

(b)CUR

Fig. 4. An external release curve of amycin and curcumin

3.3. Morphological characterization of nanoparticles after degradation

The particle size distribution of BDC after 96 h of degradation is shown in Fig. 5, (a) to (c) represent the particle size distribution of BDC after 96 h of degradation at pH=5.0, 6.0 and 7.0, respectively. It can be seen that the particle size distribution of nanoparticles was widest in PBS buffer solution at pH 5.0, intermediate at pH 6.0, and narrowest in buffer solution at pH 7.0. The wider particle size distribution with increasing acidity indicated that the release was more complete, which might be due

to the breaking of the enol ether bond in the BDC, while the particle size distribution of nanoparticles in the simulated physiological environment at pH 7.0 did not change significantly from that before the slow release.

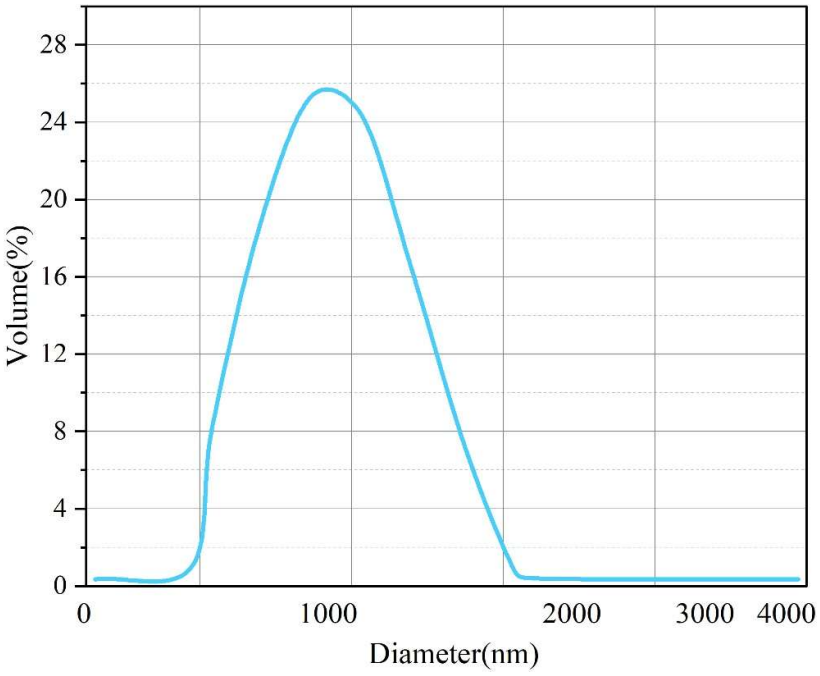

(a)pH=5.0

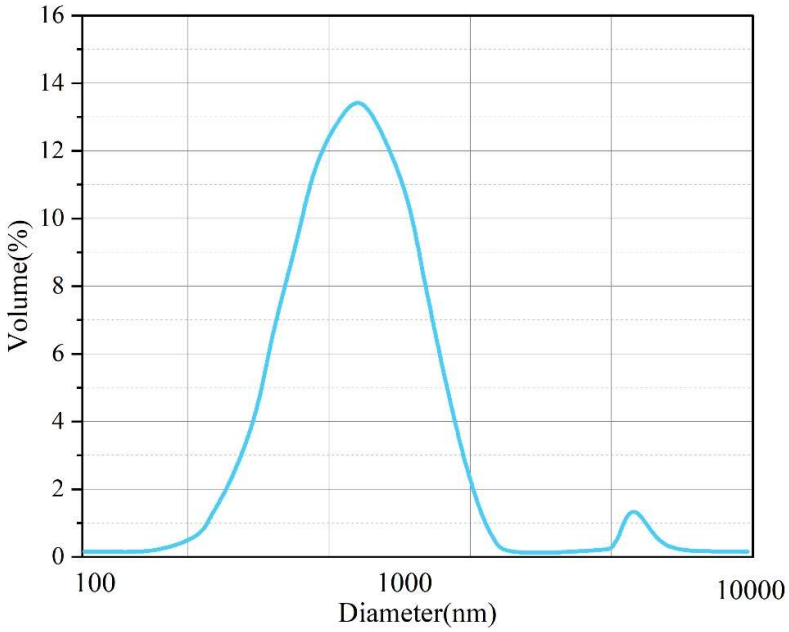

(b) pH=6.0

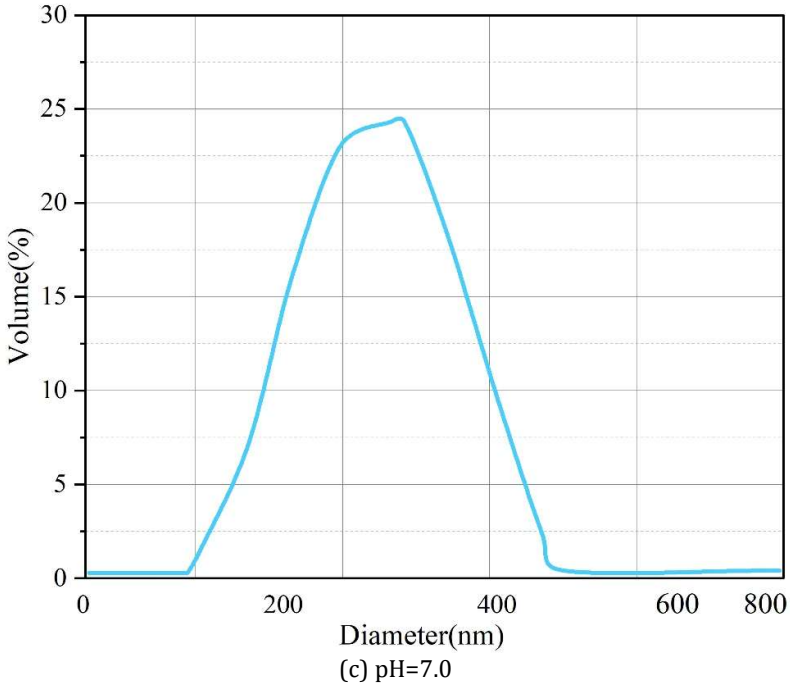

(c) pH=7.0

Fig. 5. The distribution of the diameter of the BDC after the degradation of 96h

3.4. Determination of the optimal preparation process

Based on the parameter optimization analysis of the constructed model by Design-expert software, the optimal preparation process was obtained as 13.15:1 (mg/mg) for the mass ratio of soybean phospholipids to drug, 4.08:1 (mg/mg) for the mass ratio of soybean phospholipids to cholesterol, and the sonication time of 30 min, which resulted in a predicted particle size of 198.34 nm and a drug loading of 10.87%. Three batches of DOX nanoliposomes were prepared in parallel according to the above optimal preparation process for validation. The results of the validation of the optimal preparation process are shown in Table 1; the results of the particle size distribution are shown in Figure 6. It was found that the measured values were in good agreement with the predicted values, suggesting that the optimized preparation process was simple and feasible, and the particle sizes conformed to normal distribution.

Three batches of DOX nanoliposomes were prepared in parallel according to the above optimal preparation process for validation. The measured value of the particle size was 200.72, and the drug loading capacity was 11.03%, which was in good agreement with the predicted value, suggesting that the optimized preparation process was simple and feasible, and the particle size conformed to normal distribution.

In this study, the preparation process of DOX nanoliposomes was optimized by using the experimental method of albumin drug-loaded nanoparticles, and the optimized process was 13.15:1 (mg/mg) for the mass ratio of soya bean phospholipids to drug, 4.08:1 (mg/mg) for the mass ratio of soya bean phospholipids to cholesterol, and the ultrasonic time was 10 min. The particle size of DOX nanoliposomes obtained by the optimized process was 200.72 nm, and the drug-loading capacity was 11.03%, which showed good agreement with the prediction. The DOX nanoliposomes obtained by this optimized process had a particle size of 200.72 nm and a drug loading capacity of 11.03%, which made the process simple and feasible. The results of the photothermal conversion test showed that the DOX nanoliposomes had concentration- and time-dependent photothermal conversion effects, which can provide a reference for further research on the near-infrared light-responsive tumor-targeted drug delivery carriers.

Table 1. Optimal preparation process verification results

Index	Predictive value	Measured value	Relative error (%)
Particle size (nm)	198.34	200.72	2.38
Amount of medicine (%)	10.87	11.03	0.16

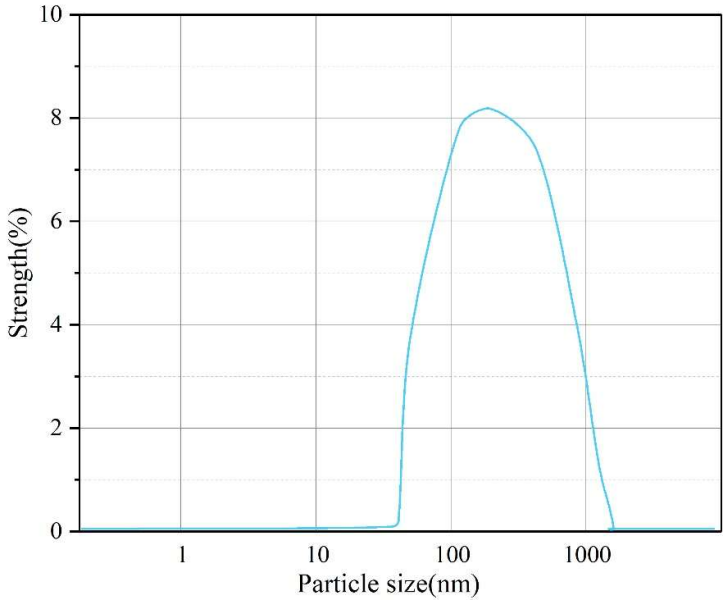

Fig. 6. The result of particle size distribution

3.5. Photothermal conversion experiments with DOX nanoliposomes

Photothermal conversion test of DOX nanoliposomes was carried out with reference to relevant literature. DOX nanoliposomes were taken and diluted with water to make nanosuspensions of copper sulfide nanoparticles with mass concentrations of 0.1, 0.2 and 0.4 mg/mL. Take 3 mL of the above nanosuspension respectively, put it in a quartz colorimetric cell, irradiate it (excitation wavelength: 808 nm) with a laser (2.5 w/cm2), and record the value of the temperature change with time every 30 s. With water as the control group, time as the horizontal coordinate and temperature as the vertical coordinate, the photothermal conversion curve is shown in Figure 7. The temperature of DOX nanoliposomes containing different mass concentrations of copper sulfide nanoparticles under 808 nm laser irradiation can rise significantly with the extension of irradiation time, and the higher the concentration the faster the temperature rise. When the irradiation time is 8min, the temperatures of copper sulfide nanoparticles with mass concentrations of 0.1, 0.2 and 0.4 mg/mL are 46.22, 49.88 and 53.01℃, respectively, and the temperature of ultrapure water is basically unchanged at this time, which is maintained at 24.54℃. It can be seen that DOX nanoliposomes have concentration- and time-dependent photothermal conversion effects, which can be combined with near-infrared laser irradiation for PTT treatment.

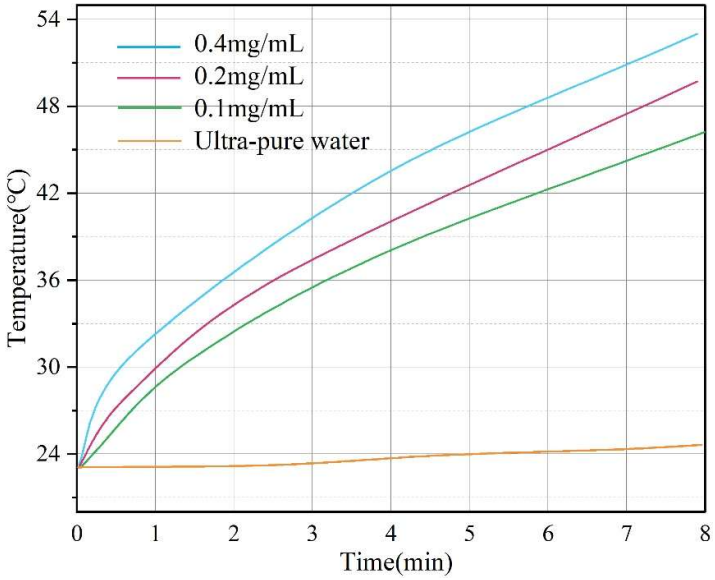

Fig. 7. Photothermal conversion curve

3.6. Characterization of optical properties

In order to confirm that the upconverted UV light can excite PFNSNO for photodynamic therapy and NO release through the fluorescence resonance energy transfer process, we tested the absorption spectra of PFNSH and UCNP@PFNSNO and the emission spectra of UCNP, respectively.

The absorption spectra of PFNSH and the emission spectra of UCNP are shown in Fig. 8, and the absorption spectra of UCNP@PFNSNO and the emission spectra of UCNP are shown in Fig. 9. The absorption spectra of PFNSH as well as UCNP@PFNSNO and the upconversion UV emission spectra of UCNP overlap well, which provides the necessary conditions for the effective energy transfer process to occur between them. Meanwhile, we also detected the changes of fluorescence emission spectra before and after PFNSNO-coated UCNP. The fluorescence spectra of UCNP before and after PFNSNO-coated UCNP under 365 nm photoexcitation are shown in Fig. 10; and the fluorescence spectra of UCNP before and after PFNSNO-coated UCNP under 365 nm photoexcitation are shown in Fig. 11. From the figure, it can be seen that the emission spectra of UCNP between 250 and 400 nm had a great fluorescence burst after coating, however, the emission spectra between 430 and 480 nm did not have a great change, which reinforces the fact that energy transfer can occur between UCNP and PFNSNO. When excited with 365 nm light, the emission spectra of PFNSNO and UCNP@PFNSNO were essentially unchanged, which indicates that the presence of UCNP does not affect the optical behavior of PFNSNO itself.

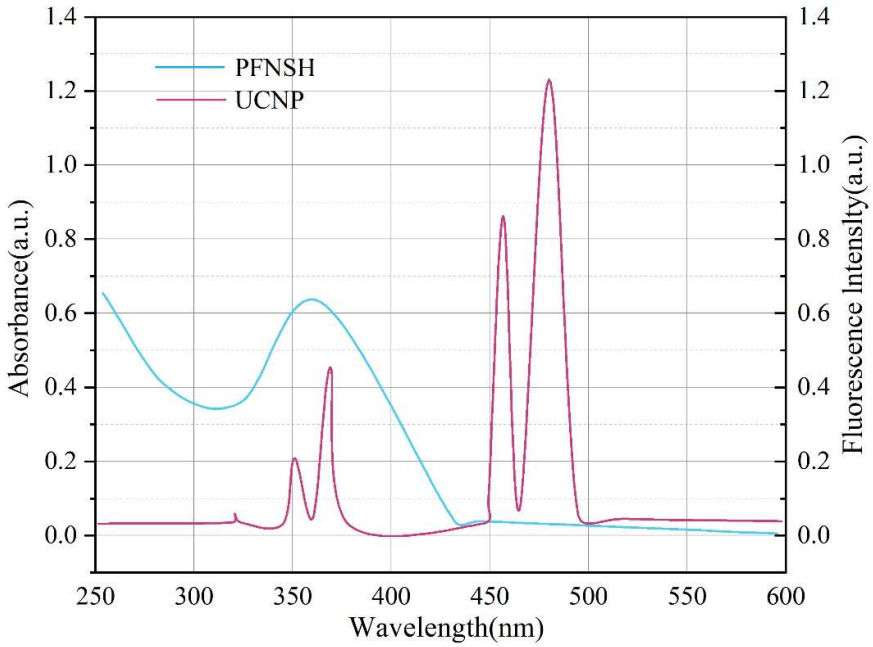

Fig. 8. PFNSH absorption spectrum and CNP emission spectrum

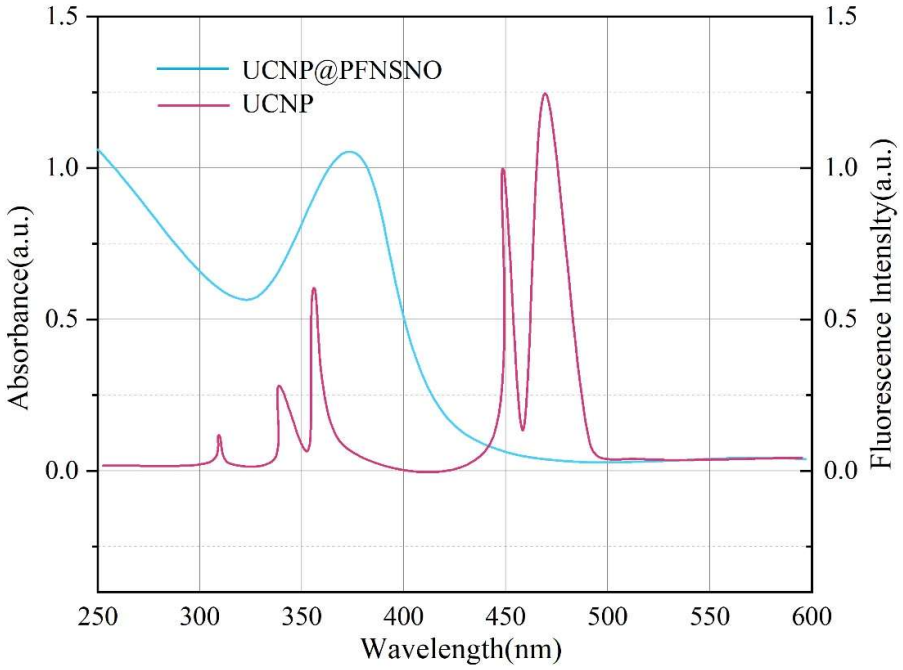

Fig. 9. The absorption spectrum of cnp@pfnsno and the emission spectrum of CNP

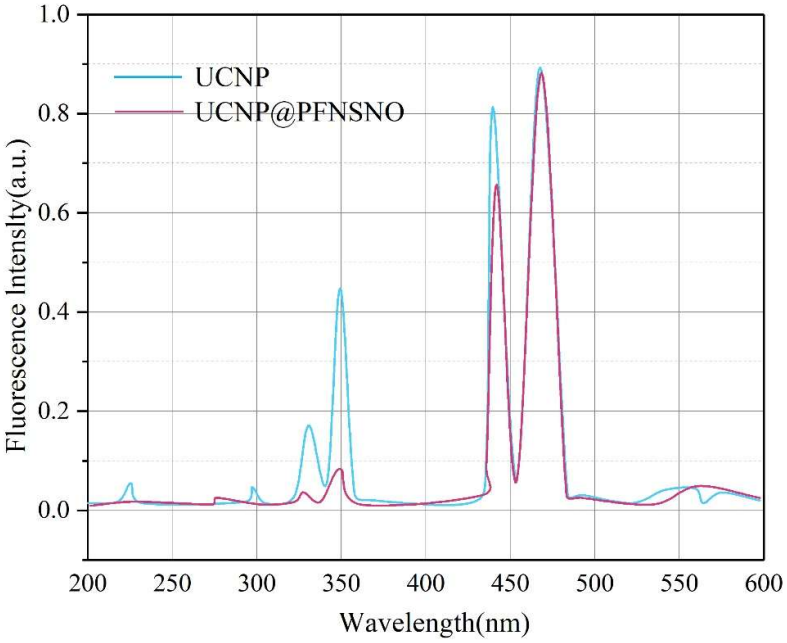

Fig. 10. CNP is modified by the fluorescence spectrum of the pfnsno envelope

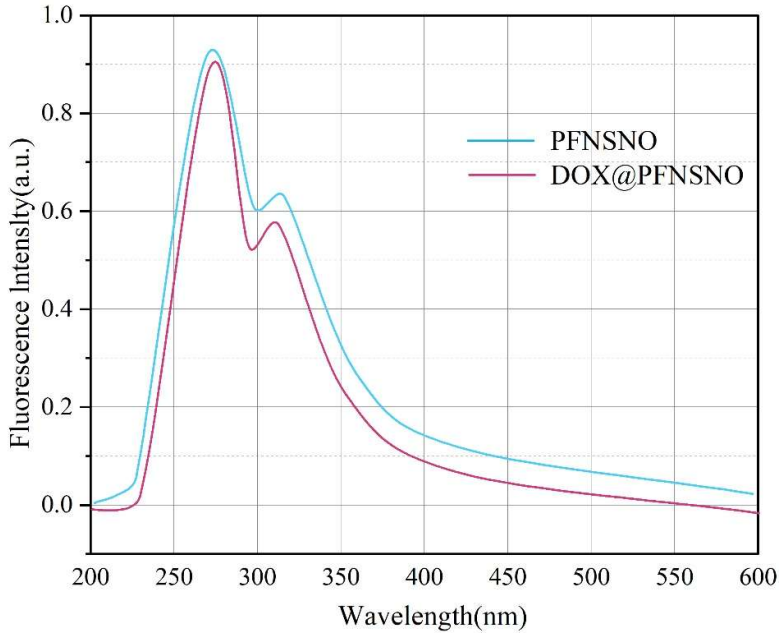

Fig. 11. Pfnsno encapsulation of CNP fluorescence spectra

4. Conclusion and outlook

4.1. Conclusion

In this study, experiments on albumin-loaded drug nanoparticles were carried out under the numerical simulation calculation method to test and discuss the performance of near-infrared photothermal-controlled nano-retarded-release system loaded with adriamycin.

The experimental simulation results show that the thermal response rate and drug release efficiency under the NIR photothermal controlled nano-retarded release system can be significantly affected by adjusting the photothermal conversion efficiency of the nanomaterials. The optimized nano-systems showed good in vitro release performance in in vitro tests, and it was found that the

trend of the retardation curves of different drugs was basically the same, and their cumulative release rates were significantly dependent on both pH and time. In addition, DOX nanoliposomes have concentration- and time-dependent photothermal conversion effects. It can be combined with near-infrared laser irradiation for PTT treatment. In addition, the converted UV light was able to excite PFNSNO for photodynamic therapy as well as NO release through the fluorescence resonance energy transfer process, and was found to be able to undergo energy transfer between UCNP and PFNSNO. It can be seen that the self-assembled albumin drug-carrying nanoparticles proposed in this paper can continuously release adriamycin under near-infrared light irradiation and effectively inhibit the growth of tumor cells, which has a good application prospect.

4.2. Outlook

4.2.1. Integrated development of multimodal imaging and therapy. Future research can combine the numerical simulation technology-optimized loaded adriamycin near-infrared photothermally controlled nano-slow-release system with multimodal imaging technology to achieve precise localization, real-time monitoring and efficient treatment of tumors. By introducing magnetic materials, fluorescent dyes and other imaging probes into the nano-system, and using magnetic resonance imaging, computed tomography, positron emission tomography and other imaging means, the morphology, metabolism, and blood flow of the tumor tissue can be observed in real time, and the irradiation position, intensity, and time of NIR light can be guided, so as to make the release of adriamycin more accurately focused on the tumor area, improve the therapeutic effect, and reduce the normal tissue damage to normal tissues.

4.2.2. Development of personalized treatment plans. With the powerful data processing and analysis capabilities of numerical simulation computing, it is expected that in the future, personalized treatment plans will be tailored to each patient according to his or her tumor characteristics, gene expression, physiological state and other factors. By simulating the drug release behavior, heat distribution and tumor cell response of nanosystems under different parameters, the therapeutic effect will be predicted, so as to optimize the composition and structure of nanosystems and the parameters of near-infrared light irradiation, and to realize precision medicine.

4.2.3. Combinations with other treatments. The combined application of near-infrared photothermal controlled nano-mitigation system loaded with adriamycin with other anti-cancer treatments such as radiotherapy, chemotherapy and immunotherapy is expected to produce a coordinated effect and improve the therapeutic effect. For example, during radiotherapy, the nanosystem can be used as a sensitizer to enhance the sensitivity of tumor cells to radiation; when combined with immunotherapy, the photothermal effect and drug release of the nanosystem can activate the immune system and enhance the body's immune response to tumors.

4.2.4. Exploration and Application of Novel Nanomaterials. Novel nanomaterials are continuously being explored and developed to improve the performance of near-infrared photothermal controlled nano-retarded release systems for adriamycin. For example, nanomaterials with higher photothermal conversion efficiency, better biocompatibility and lower toxicity are being investigated to enable the system to warm up more rapidly and stably under NIR light irradiation for efficient release of adriamycin. Also, the introduction of novel materials can help improve the targeting of the system so that it can deliver the drug more accurately to tumor tissues.

Funding

This work was supported by Major Project of Henan Province Higher Education Teaching Reform Research and Practice Project for the year 2024 (Project Number: 2024SJGLX0634).

References

[1] Kim, B. H., & Park, J. W. (2017). Epidemiology of liver cancer in South Korea. Clinical and molecular hepatology, 24(1), 1.

[2] Anwanwan, D., Singh, S. K., Singh, S., Saikam, V., & Singh, R. (2020). Challenges in liver cancer and possible treatment approaches. Biochimica et Biophysica Acta (BBA)-Reviews on Cancer, 1873(1), 188314.

[3] Rumgay, H., Arnold, M., Ferlay, J., Lesi, O., Cabasag, C. J., Vignat, J., ... & Soerjomataram, I. (2022). Global burden of primary liver cancer in 2020 and predictions to 2040. Journal of hepatology, 77(6), 1598-1606.

[4] Yu, M., & Li, S. (2022). Irreversible electroporation for liver cancer ablation: A meta analysis. European Journal of Surgical Oncology, 48(6), 1321-1330.

[5] Raoul, J. L., Forner, A., Bolondi, L., Cheung, T. T., Kloeckner, R., & de Baere, T. (2019). Updated use of TACE for hepatocellular carcinoma treatment: How and when to use it based on clinical evidence. Cancer treatment reviews, 72, 28-36.

[6] Izzo, F., Granata, V., Grassi, R., Fusco, R., Palaia, R., Delrio, P., ... & Curley, S. A. (2019). Radiofrequency ablation and microwave ablation in liver tumors: an update. The oncologist, 24(10), e990-e1005.

[7] Chen, Q., Shang, W., Zeng, C., Wang, K., Liang, X., Chi, C., ... & Tian, J. (2017). Theranostic imaging of liver cancer using targeted optical/MRI dual-modal probes. Oncotarget, 8(20), 32741.

[8] Quinto, A. M., Nutu, O. A., Manso, R. S. R., Alonso, I. J., Pulido, J. C., Municio, A. M., ... & Romero, L. C. J. (2018). Complications of transarterial chemoembolization (TACE) in the treatment of liver tumors. Cirugía Española (English Edition), 96(9), 560-567.

[9] Zou, H., Wang, F., Zhou, J. J., Liu, X., He, Q., Wang, C., ... & Xiong, L. (2020). Application of photodynamic therapy for liver malignancies. Journal of gastrointestinal oncology, 11(2), 431.

[10] Kaibori, M., Kosaka, H., Matsui, K., Ishizaki, M., Matsushima, H., Tsuda, T., ... & Sekimoto, M. (2021). Near-infrared fluorescence imaging and photodynamic therapy for liver tumors. Frontiers in oncology, 11, 638327.

[11] Mintz, K. J., & Leblanc, R. M. (2021). The use of nanotechnology to combat liver cancer: Progress and perspectives. Biochimica et Biophysica Acta (BBA)-Reviews on Cancer, 1876(2), 188621.

[12] Sharma, A., Cressman, E., Attaluri, A., Kraitchman, D. L., & Ivkov, R. (2022). Current challenges in image-guided magnetic hyperthermia therapy for liver cancer. Nanomaterials, 12(16), 2768.

[13] Chen, Y. C., Chiu, W. T., Chang, C., Wu, P. C., Tu, T. Y., Lin, H. P., & Chang, H. C. (2018). Chemo-photothermal effects of doxorubicin/silica–carbon hollow spheres on liver cancer. RSC advances, 8(64), 36775-36784.

[14] Liu, X., Zhou, W., Wang, T., Miao, S., Lan, S., Wei, Z., ... & Fan, H. (2023). Highly localized, efficient, and rapid photothermal therapy using gold nanobipyramids for liver cancer cells triggered by femtosecond laser. Scientific Reports, 13(1), 3372.

[15] Kabiri, S., & Rezaei, F. (2022). Liver cancer treatment with integration of laser emission and microwave irradiation with the aid of gold nanoparticles. Scientific Reports, 12(1), 9271.

[16] Huang, M., Qi, M., Yang, H., Peng, Z., Chen, S., Liang, M., ... & Hu, M. (2023). Noninvasive Strategies for the Treatment of Tiny Liver Cancer: Integrating Photothermal Therapy and Multimodality Imaging EpCAM-Guided Nanoparticles. ACS Applied Materials & Interfaces, 15(18), 21843-21853.

[17] Burrini Nastassja,D'Ambrosio Mario,Gentili Matteo,Giaquinto Roberta,Settimelli Veronica,Luceri Cristina... & Francesconi Oscar. (2023). Niosomes Functionalized with a Synthetic Carbohydrate Binding Agent for Mannose-Targeted Doxorubicin Delivery. Pharmaceutics(1),235-235.

[18] Yosub Ha,Seongha An & Seung R Paik. (2024). Combination of Chemical and Physical Cancer Therapeutics

Developed with Microcapsules Made of κ-Casein and Gold Nanoparticles in the Presence of Drug-Loaded Phase Change Materials.. ACS applied materials & interfaces

[19] Junyi Yang,Rule Deng,Song Jia,Yang Wang & Xuefei Wang. (2024). UV-Vis spectrophotometric determination of isoprene in atmosphere based on Diels–Alder reaction. International Journal of Environmental Analytical Chemistry(20),9117-9127.